



## Democratising dry adhesion development with consumer-grade AM

Vegar Stubberud , Martin Steinert and Håkon Jarand Dugstad Johnsen

Norwegian University of Science and Technology, Norway

 Vegar.stubberud@ntnu.no

### Abstract

The production of reusable gecko-inspired dry adhesives has traditionally been done with complex nanofabrication methods such as lithography and PDMS casting. This article presents a way of producing and testing dry adhesive samples using consumer-grade AM machines and equipment typically available in a Makerspace. The samples produced exhibit adhesive properties depending on the preload and surface structure, and we conclude that consumer-grade AM is suitable for rapid prototyping and testing of dry adhesion. However, it is limited by the scale and accuracy compared to traditional methods.

*Keywords: additive manufacturing, biomimicry (biomimetics), dry adhesion, open source design, 3D printing*

## 1. Introduction

The gecko is a lizard capable of adhering to surfaces with varying roughness. This adhesion effect results from hierarchical structures of a compliant matter on the gecko's toe pad called setae (Tricinci et al., 2018). These hierarchical structures exist in the number of thousands on each toe and terminate in pads of micro- and nanoscale (Tian et al., 2006). The conformal nature of these structures facilitates a large sum of contact area, resulting in van der Waals forces between the structures and the surface (Autumn et al., 2002), keeping the gecko attached. This remarkable way of adhering to surfaces has inspired many attempts at recreating and approximating what is often called "dry adhesion" or "gecko adhesion". Dry adhesion is reusable and leaves no residue and has the potential to replace other traditional adhesives where reusability is key, such as in space applications or in pick-and-place machines. Traditional nanofabrication methods, such as lithography and PDMS casting, have often been used for producing dry adhesives, reducing the complex geometry of the gecko's setae into simpler shapes (del Campo et al., 2007; Davies et al., 2009; Jin et al., 2012, 2014; Yu et al., 2012; Zhang et al., 2016, 2021; Purtov et al., 2018). Attempts using two-photon lithography have also been made (Röhrig et al., 2012; Tricinci et al., 2018). The mentioned methods often require a cleanroom environment, costly machines, and proper training while being a time-consuming effort. The realm of consumer-grade additive manufacturing (AM) machines has not been adequately explored for the biomimicry of dry adhesion. Exemplifying the production and testing of dry adhesives via an open hardware and open-source project can aid in democratising dry adhesion into the field of consumer-grade AM. Consumer-grade AM machines mainly focus on a size scale where one can hold and interact with the objects made. With the gecko having micro- to nanometre-scale structures, the resolution and detail of what can be printed is an obvious limitation, and a direct approximation of its adhesive geometries cannot be made with today's consumer-grade machines. Attempts at dry adhesion using lithography have often simplified the gecko's adhesive structures into flexible pillars or lamellas emerging from a flat base (del Campo et al., 2007; Parness et al., 2009; Jin et al., 2012; Raut et al.,

2018). With this approach, the individual structures conform to the target surface facilitating for van der Waals forces at the contact area and shares the load at both preload and retraction. At these attempts, the dimensions of the pillars range from the sub-micrometre scale up to the sub-millimetre scale (Murphy, Kim and Sitti, 2009). Using consumer-grade Masked Stereolithography (MSLA) printers, one is mainly limited by the LCD screen's pixel size. For the Prusa SL1S, the pixel size is ca. 50x50 micrometres (Prusa, 2021), enabling the creation of structures in the sub-millimetre scale. Using an elastomeric resin resembling PDMS, one can potentially have a way of production using AM that can compete with previous attempts using lithographic methods.

## 2. Experimental methods

### 2.1. Fabrication using MSLA

The off-the-shelf BASF FL300 resin, with a typical shore A hardness of 40 (Fei et al., 2023), was chosen as it closely resembles the 44-54 shore A hardness of the common Sylgard-184 PDMS (Johnston et al., 2014). Using a resin with similar material properties as PDMS facilitates comparison to previous works implementing dry adhesion by PDMS casting. Calibration and visual inspection ensure that 1.6 s exposure time per layer in the Prusa SL1S is suitable for printing details on a sub-millimetre scale with this resin. The selected geometry for testing is presented in Figure 1, and the dimensions are listed in Table 1. The selection includes an unstructured sample with a flat surface. The base thickness for all samples was 2 mm.

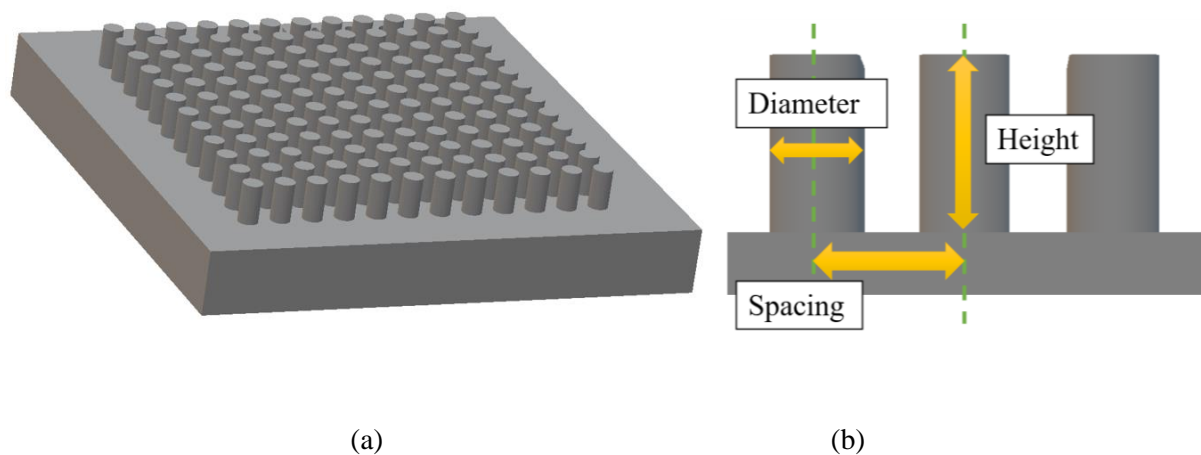


**Figure 1. Example model of a structured sample (a) and defining sample dimensions (b)**

All parts were printed with a layer height of 0.025 mm and post-processed by brushing excess resin off with a painter's brush and IPA, followed by an IPA bath with magnetic stirring for 3-4 minutes. After washing, the parts were post-cured in the Prusa wash and cure machine for 5 minutes. A set of each sample type was dip-transferred to produce a mushroom tip geometry similar to some previous works (Davies et al., 2009; Murphy, Kim and Sitti, 2009). Figure 2 presents this process and the resulting mushroom tip shape for sample  $A_{DT}$  compared to the untreated sample A. The first steps in the dip transfer consists of dipping the tips of the sample in a thin film of uncured resin (steps 1-3). The sample is then transferred to a fluorinated ethylene propylene (FEP) film (step 4), and the uncured resin is cured under UV light (step 5). The FEP film is removed to expose the mushroom tips on the sample (step 6). A FEP film is a standard replacement part in ordinary MSLA machines and is likely available in a FabLab or Makerspace.

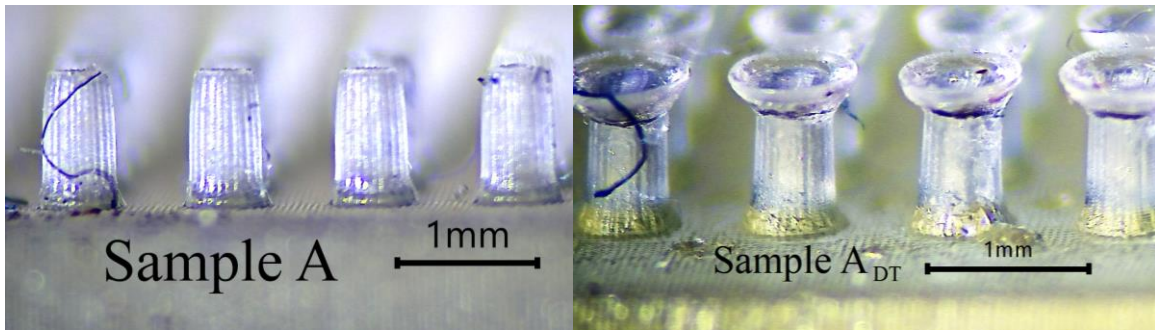
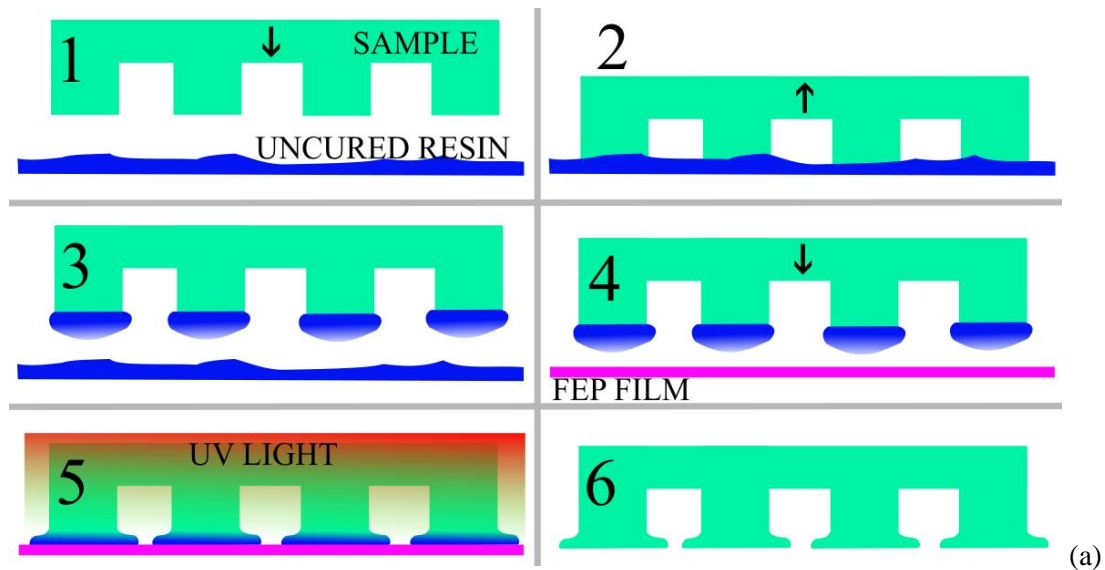


Figure 2. The dip transfer process (a) and microscope images showing the difference in resulting geometry after the dip transfer (b)

## 2.2. Test setup

Using high-end adhesion testing equipment was disregarded as this project aims to show how this development of dry adhesive can be explored cheaply and in an accessible matter within the AM realm. The Prusa MK2 was chosen as a 3-axis manipulator for moving the testing probes relative to the samples. The printer was fitted with magnetic encoders on the stepper motors of the X, Y and Z axes to measure position. The print bed was modified to include two load cells for measuring horizontal and vertical force. The force and positional data are collected by serial communication via an Arduino Nano for analysis. A Python script generated G-codes for controlling the probe's position in a down and up movement.

Two probes are selected for testing: one circular cutout of flat acrylic plastic with a diameter of 10 mm and a spherical glass marble with a diameter of 15 mm. The spherical probe is included as it represents an uneven surface and can give insights into how adhesion is affected by the shape of the target surface. In addition, the spherical probe requires no alignment to the samples. The circular flat probe is aligned visually with the surface of the sample holder. Each sample is glued on a separate 30x30 mm sheet of acrylic plastic to fit securely into the sample holder. The Prusa MK2 testing rig can be seen in Figure 3a.

A degassing chamber was used in this project to evaluate the role of vacuum-induced forces during adhesion testing. Inside it, a smaller fused filament fabrication (FFF) printer was used for positioning the probe in relation to the sample. Such a large degassing chamber is not commonly found in a normal Makerspace or FabLab. However, this test will provide a deeper understanding of the forces acting in samples produced by the methods in this project and can be used as a reference for later development

and discussion. As with the primary testing rig, this machine was equipped with magnetic encoders and Arduino for data transfer. This setup can be seen in Figure 3b.

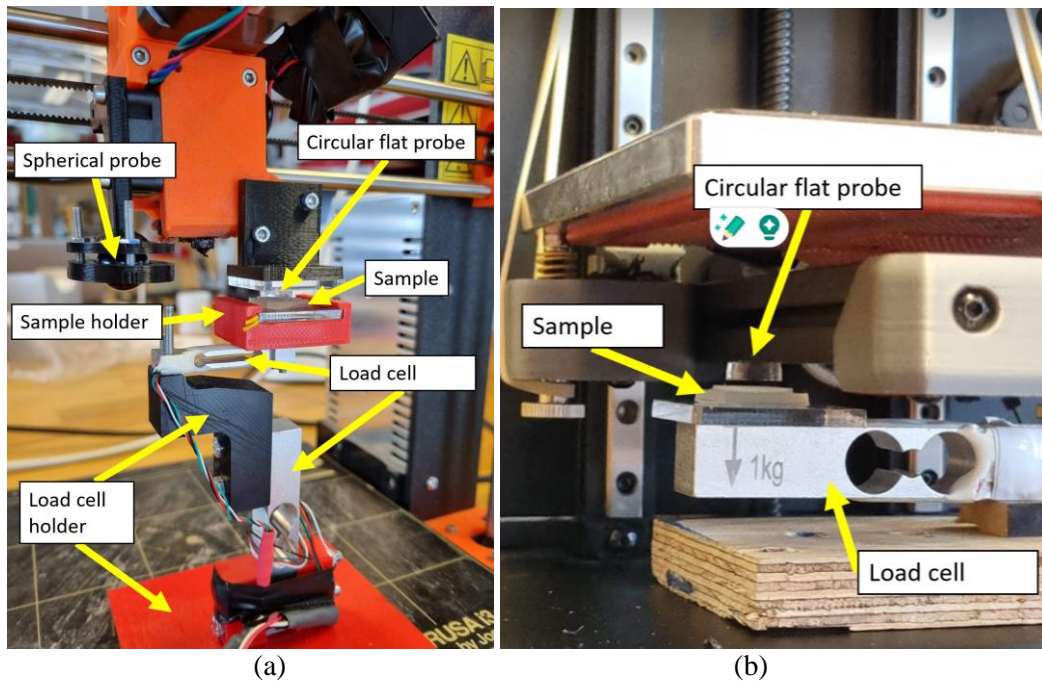


Figure 3. Test setup using Prusa FFF (a) and the test setup for low-vacuum testing (b)

### 2.3. Testing procedure

The G-code written for the testing rigs instructs the machines to move the probe downwards and upwards three times with the same Z travel. The movement is repeated with an increased Z travel of 0.1 mm for the next cycle. The number of cycles for each sample is listed in Table 1. Adhesion tests were made on all samples with the spherical and flat probe. The probes and samples were cleaned with IPA before each run. Sample A, A<sub>DT</sub> and U<sub>DT</sub> were selected for testing in low-vacuum conditions. The adhesion test for each sample was run once before inserting the machine into the degassing chamber, two times inside the chamber at -70 kPa and once inside the chamber at atmospheric pressure. The selected samples were cleaned with IPA before the first test. No cleaning was done between the first and the last test. Compression force peaks and their respective adhesion peaks are gathered for analysis. Microscope images of all samples were taken to analyse the area fraction, i.e., potential contact area divided by reference area.

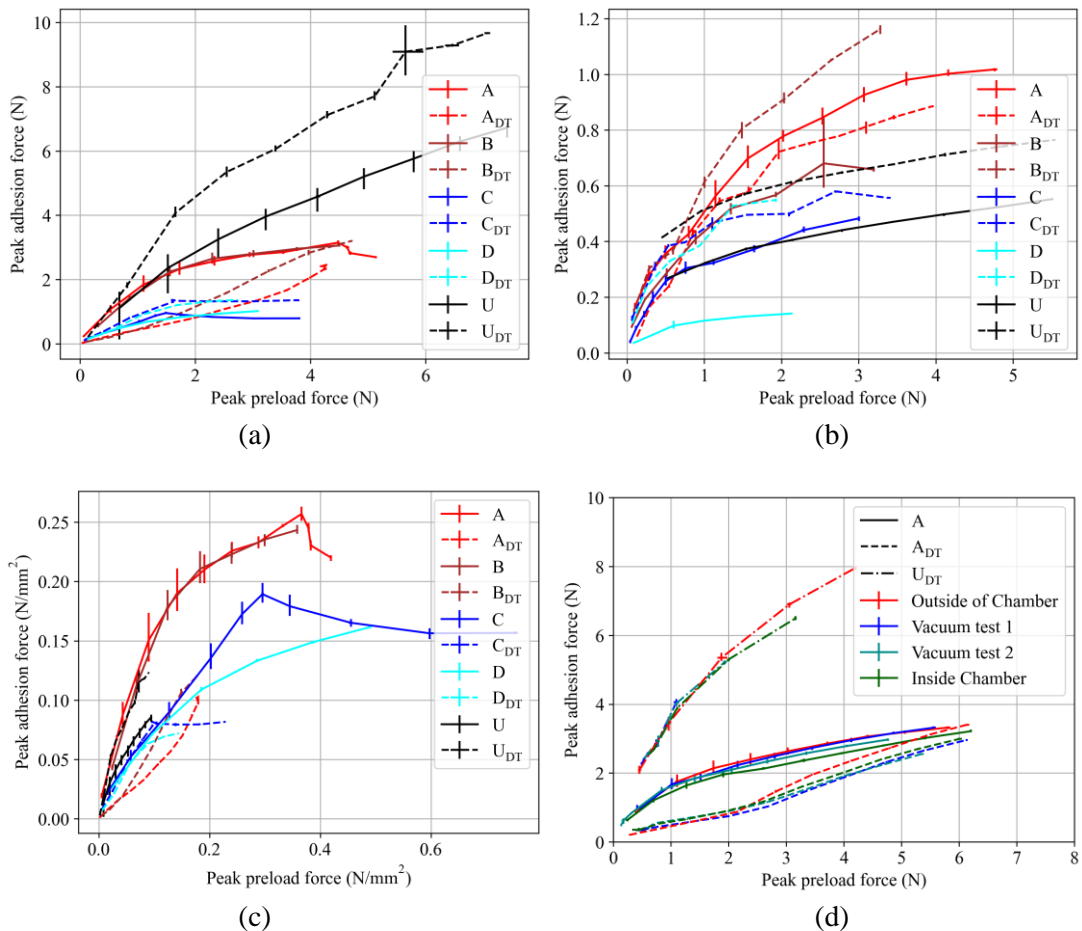
Table 1. Samples produced

Sample	Diameter (mm)	Height	Spacing	Dip transfer	Area fraction	Probing cycles	Vacuum tested
A	0.6	1.2	1	-	0.156	12	X
A <sub>DT</sub>	0.6	1.2	1	X	0.302	12	X
B	0.6	0.8	1	-	0.160	8	-
B <sub>DT</sub>	0.6	0.8	1	X	0.340	8	-
C	0.4	1	0.8	-	0.064	10	-
C <sub>DT</sub>	0.4	1	0.8	X	0.212	10	-
D	0.4	0.6	0.8	-	0.080	6	-
D <sub>DT</sub>	0.4	0.6	0.8	X	0.242	6	-
U	-	-	-	-	1	10	-
U <sub>DT</sub>	-	-	-	X	1	10	X

### 3. Results

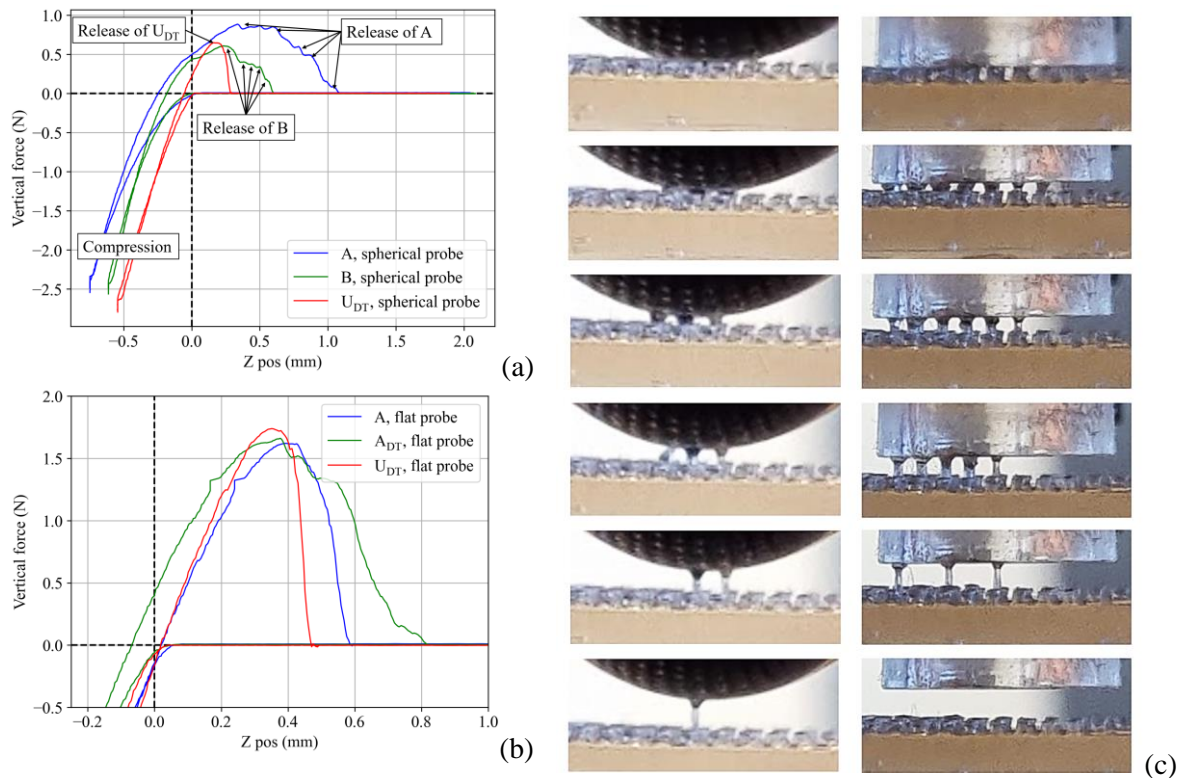
This section presents the force data collected from the adhesion tests and key observations during testing. Figure 4a and Figure 4b show the peak adhesion force vs peak preload force for the flat circular and spherical probes, respectively. Both plots indicate a trend of a stronger adhesion force at higher preloads. The error bars in all subfigures of Figure 4 represent the highest and lowest preload and adhesion values within the cycle, and the line is plotted through the average values. It is apparent that the samples  $U_{DT}$  and  $U$  provide the strongest adhesion force for the flat circular probe, while sample  $B_{DT}$  provides the strongest adhesion force for the spherical probe. Evidently, the trend of adhesion force per preload force is higher for the circular flat probe than the spherical probe.

Figure 4c shows the peak adhesion and preload adjusted for contact area, i.e., force divided by probe area and area fraction. Here, samples A and B have roughly the same initial path as the  $U_{DT}$  sample and exhibit the strongest peak adhesion per area. Data from the vacuum tests in Figure 4d show no significant difference in adhesion for the tests in atmospheric pressure compared to the ones in -70 kPa.



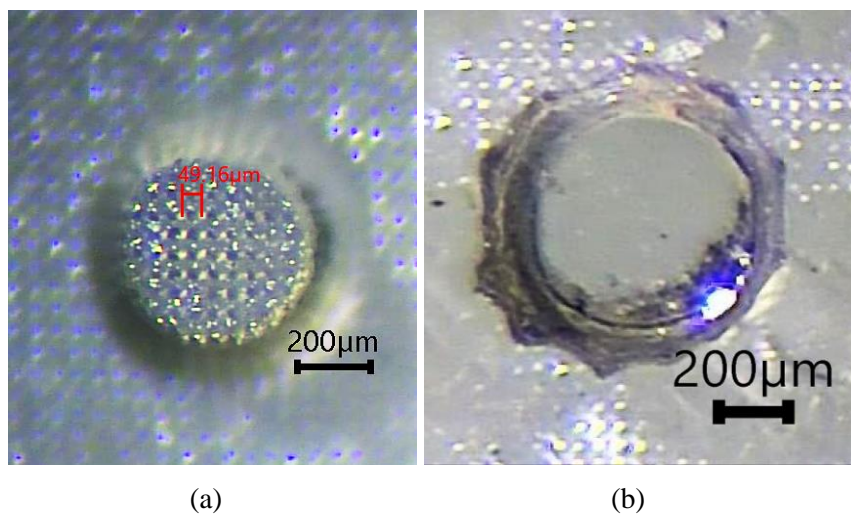
**Figure 4. Peak adhesion data for the flat circular probe (a); peak adhesion data for the spherical probe (b); peak adhesion data adjusted for contact area for the flat circular probe (c); peak adhesion data from tests in low vacuum (d)**

Figure 5c visually shows the release pattern of sample  $B_{DT}$  on the spherical and flat probe. The cylinders stretch beyond their initial position and release one by one. The plot of Figure 5a shows the vertical force over a single down and up movement for samples A, B and  $U_{DT}$  with a spherical probe with ca. the same preload. This graph shows the gradual release of the sample when the spherical probe retracts. The most apparent release points are marked with arrows. The plot in Figure 5b shows the release of sample A,  $A_{DT}$  and  $U_{DT}$  with ca. the same peak adhesion with the flat probe.



**Figure 5. Vertical force over distance for a single release of sample A, B, U<sub>DT</sub> with the spherical probe (a); vertical force over distance for a single release of sample A, A<sub>DT</sub> and U<sub>DT</sub> for the flat probe (b); the release of sample B<sub>DT</sub> from the spherical and flat circular probe (c)**

The surface geometry on the raw printed samples had bumps in the surface in a grid pattern where the spacing between the tops equals the pixel size, i.e., ca. 50 microns. This is seen in Figure 6a. The samples that were dip transferred had a surface quality matching the one of the FEP film used for dip transfer. This surface was observed under the microscope to be smooth and without any marks, as seen in Figure 6b. During testing with the Prusa rig and the vacuum rig, observations of the compliance of the testing rigs were made. Both rigs show a significant flex from the probe to the sample holder.



**Figure 6. Microscope image of sample B (a) and sample B<sub>DT</sub> (b)**

## 4. Discussion

The data gathered indicate that adhesion is present and dependent on the amount of preload for all combinations of probes and samples. The compliance observed means that the entire test rig can be modelled as a spring system from the sample holder through the rig up to the probe. However, since the sample holder's placement on the test rig was not identical for each test run, the compliance was not equal for all tests. Because of this, the recorded Z position during compression and retraction cannot be used as an accurate position measurement for data analysis. The peak adhesion and preload forces, however, will still be adequate for analysis as the forces measured still represent the forces acted on the sample by the probe. With the aim of presenting a low-cost approach to producing and testing dry adhesion, the search for a more rigid testing rig was not done as the chosen rig based on the Prusa FFF printer is so widely available.

### 4.1. Adhesion properties

The flat probe, providing all its potential contact area at the initial contact, displays the strongest adhesion with samples U and  $U_{DT}$ . This is expected as the unstructured samples have the highest area fraction and can potentially create van der Waals forces over the entire probe area. With the flat probe, the potential contact area of the probe is fixed at  $78.5 \text{ mm}^2$ . One can, therefore, divide the force values by the area fraction to get the force values per unit of potential contact area. This allows for examining how different surface structures affect the potential adhesion in this test. For the area-adjusted data, samples A and B show the highest peak adhesion per area. Their dip-transferred counterparts show a lower adhesion as the dip-transfer process increased the area fraction without proportionately increasing the peak adhesion.

The spherical probe exposes a larger contact area the further it is compressed into the sample. With a low amount of compression, the tips align themselves to be parallel to the surface of the sphere. When the probe is compressed into the sample, individual contact points appear on different z-levels of the probe. As a consequence of this, each pillar will be released at different times during the retraction of the probe. This effect can be seen in Figure 5a, where the release is stepwise rather than smooth for samples A and B. Comparing this to the unstructured samples, they practically have a single area of contact and will experience a peeling effect during retraction. It will mainly be the lowest part of the spherical probe that creates the peak adhesion, and the release is fast rather than gradual, like for the structured samples. This rapid release is apparent in Figure 5a.

An apparent advantage of having a structured surface with individual contact points is that they release independently of each other and that they can stretch. Each pillar in the adhesion system contributes with its individual mechanical and adhesion properties. The release of a single pillar causes a redistribution of load to the others instead of an almost instant peeling, as for the unstructured samples. This is especially beneficial for a target surface such as the spherical probe, as the peeling effect is more prominent on non-planar surfaces for the unstructured samples. This can explain the performance difference for the unstructured samples compared to the rest of the samples when changing from the flat probe to the spherical.

The manual process of dip transfer resulted in a somewhat varying tip area for the treated samples. For the flat probe, this varying tip area may cause the pillars to release at different expansion levels instead of a homogenous release at the same expansion. This may be the cause for the lower peak adhesion force for many of the dip-transferred samples with a flat probe. With the untreated samples, the structures are relatively homogenous, resulting in a synchronous buildup of tension and release at the same expansion, causing a high peak adhesion compared to the structures that release gradually without the same buildup of tension. This can be seen in the plot of Figure 5b, as it is apparent that sample A releases more rapidly than sample  $A_{DT}$ . This plot also exemplifies the almost instant release of the  $U_{DT}$  sample as it acts like a single pillar releasing.

The dip-transferred samples generally perform better than their untreated counterparts with a spherical probe. This can be explained by how the contact points attach at different Z heights on the probe. Therefore, the adhesion is less dependent on a synchronous buildup of tension but rather the adhesion

of the individual pillars. Sample A<sub>DT</sub> did have lower peak adhesion than sample A. This may result from poor-quality dip transfer in the area of contact or other factors, such as the cleaning procedure.

The structure on the raw untreated prints seen in Figure 6a may contribute to another level of hierarchy. This can influence the adhesion, but since the dip-transferred samples were not homogenous in tip area, they cannot be compared for the flat probe, and no conclusions can be made concerning this extra level of hierarchy.

The pairs of untreated samples with the same diameter, i.e., samples A and B and samples C and D, show similar adhesion properties for the flat probe since the entire area is exposed at the initial probe contact, and the contact area is the same regardless of the pillar height. For the spherical probe, however, taller structures allow the probe to reach further into the sample before hitting the base, allowing a greater surface area to be exposed, in addition to creating a greater preload on the pillars hitting the bottom part of the probe. Both the larger contact area and the higher preload on some pillars likely contribute to the increased peak adhesion. This observed increase in peak adhesion suggests that a structured sample with taller pillars conforms and adheres better to non-planar surfaces, such as the spherical probe. The same logic applies to having structured vs. non-structured adhesion surfaces for applications where the target surface is not smooth and flat.

The base of all samples, including the unstructured sample, had a thickness of 2 mm and was of the same material as the structures examined. Such a thick base will influence the data as it will contribute to the sample's conformity to the target surface. For the structured samples, this was minimised by limiting the depth of the compression to the pillar's height. For the unstructured samples, however, the elasticity and softness of the material allowed the base to conform to the probe, creating a larger contact area. This is especially relevant for the spherical probe. The considerable thickness and the soft material may influence the adhesion values for the unstructured samples.

The tests performed in the low-vacuum conditions of -70 kPa show no significant difference in peak adhesion. Looking at the geometry of the dip-transferred samples in Figure 2 and on the image series from a single release in Figure 5c, there is a visual resemblance of a suction cup on each pillar. If they acted like suction cups, one would expect lower adhesion values at lower pressures. However, this aspect can be disregarded since there is no significant difference in peak adhesion at lower pressures. For all tests, the samples and probes were cleaned with IPA to remove any residue on the surface that may cause capillary forces. Therefore, the adhesion measured in this project can be assumed to mainly be caused by the van der Waals forces in the contact area between the sample and the probe.

## 4.2. Discussion of consumer-grade AM for dry adhesion

Except for the degasser, the presented production and testing setup is based on equipment that typically exists in a FabLab or Makerspace and low-cost components available for consumers online. In this project, the vacuum tests demonstrate that the presented samples exhibit mainly van der Waals forces and can act as a reference and motivation for further dry adhesion testing using AM, as it is a common misconception that vacuum-induced forces are the primary adhesion source. The machines used require no extensive training or certification to operate, and all modifications made to the FFF printer were minor and easily reversible. The Prusa MK2 and the Prusa SL1S are in the upper price range for a hobbyist, but cheaper options exist. Comparing this low-cost AM setup to, e.g., lithographic methods used for producing similar dry adhesives, the setup presented allows for a broader community to rapidly prototype and test dry adhesion. Obviously, using traditional methods such as lithographic methods allow for a much better resolution at the cost of a time-consuming and expensive production. Using probes mounted on the extruder for adhesion testing and attaching the sample holder to the print bed turned out to cause compliance in the system. In hindsight, attaching the probes close to the Z-axis lead screw and mounting the samples in close relation to the axis would probably reduce the compliance observed. A similar testing setup could also be made with a single stepper motor and linear rails. With the presented AM-based production and testing setup, one could go from a 3D model to a printed sample and testing within an hour. This facilitates rapid prototyping with different resins, geometries, and probes much faster than traditional methods. The recorded data, wiring schematics, python code, 3D models and images of the setup will be made available to the public via GitHub to help guide those interested in this production and test method using AM. This article only presents a basic set of



geometries and testing with a single resin type. Using AM allows for a much wider set of possible geometries and materials to test, and that should be a subject for further research. Overexposing the final layer of the print may also create a tip surface similar to the dip-transferred samples since the resin may cure fully down to the FEP film and match its surface roughness instead of a bumpy pattern, as seen in Figure 6a. The Prusa SL1S used in this project does not support the option to adjust the exposure time for each layer, but some other consumer-grade MSLA printers can.

Comparing the adhesion from this approach to the gecko's is not one-to-one as the gecko's footpads are directional, meaning that the adhesion values are dependent on direction and angle of pull (Tian et al., 2006). However, when measuring the pull of force with proper preloading, the gekko gecko lizard can produce ca 100 kPa adhesion (Irschick et al., 1996; Autumn et al., 2000). The adhesion presented here are created for perpendicular preload and pull to the target surface. Dividing the adhesion force by area of the flat circular probe, sample A and B produces ca. 10 kPa of adhesion. Directly comparing the adhesion values to other dry adhesion surfaces is not straightforward as it is dependent multiple factors such as material properties, target surface and geometry. Davies et al. presents a comparison of different microstructures where the force per surface area of adhesive film varies from ~1 kPa to ~24 kPa. The length of the microstructures were 24  $\mu\text{m}$  to 100  $\mu\text{m}$  with tip diameter of 7  $\mu\text{m}$  to 40  $\mu\text{m}$  (Davies et al., 2009). These structures are considerably smaller than what is presented in this project, however, they perform in the range that are comparable our adhesion results. Smaller and denser structures will conform differently on different surfaces and will perhaps conform better to rougher surfaces, however, that will depend on the shape of the structures and the material properties among other factors. The adhesives developed here were not excessively optimized in structure size or pillar density and aims to present a starting point for further research in using consumer-grade AM for dry adhesion development.

## 5. Conclusion

The case presented in this article exemplifies how consumer-grade off-the-shelf components and AM machines with minimal modifications can be used for the development and testing of dry adhesion, which traditionally has been heavily based on nanofabrication methods such as lithography and PDMS casting combined with high-end testing equipment. As presented, this low-cost approach has weaknesses in terms of production accuracy and the compliance of the testing rig. However, it was adequate for producing various samples and recording data to evaluate the differences in adhesion performance depending on the sample's geometry and target surface. Democratizing the development of dry adhesion by using consumer-grade AM machines and components allows for a broader range of creators to develop this concept and method further. Experiments show that the samples produced adhere to the probes and that the peak adhesion depends on the preload. Structured dip-transferred samples generally exhibit the strongest peak adhesion on the spherical probe, and the structured non-dip-transferred samples exhibit the strongest peak adhesion per area on the flat probe. The role of vacuum-induced forces was examined and determined to be non-significant for the adhesion of a selection of samples that represent the geometry of the rest. The adhesion performance is within the range of other attempts at dry adhesion; however, a direct comparison is not appropriate.

## References

- Autumn, K. et al. (2000) 'Adhesive force of a single gecko foot-hair', *Nature*, 405(6787), pp. 681–685. Available at: <https://doi.org/10.1038/35015073>.
- Autumn, K. et al. (2002) 'Evidence for van der Waals adhesion in gecko setae', *Proceedings of the National Academy of Sciences*, 99(19), pp. 12252–12256. Available at: <https://doi.org/10.1073/pnas.192252799>.
- del Campo, A. et al. (2007) 'Patterned Surfaces with Pillars with Controlled 3D Tip Geometry Mimicking Bioattachment Devices', *Advanced Materials*, 19(15), pp. 1973–1977. Available at: <https://doi.org/10.1002/adma.200602476>.
- Davies, J. et al. (2009) 'A practical approach to the development of a synthetic Gecko tape', *International Journal of Adhesion and Adhesives*, 29(4), pp. 380–390. Available at: <https://doi.org/10.1016/j.ijadhadh.2008.07.009>.
- Fei, J. et al. (2023) 'Progress in Photocurable 3D Printing of Photosensitive Polyurethane: A Review', *Macromolecular Rapid Communications*, 44(18), p. 2300211. Available at: <https://doi.org/10.1002/marc.202300211>.
- Irschick, D.J. et al. (1996) 'A comparative analysis of clinging ability among pad-bearing lizards', *Biological Journal of the Linnean Society*, 59(1), pp. 21–35. Available at: <https://doi.org/10.1111/j.1095-8312.1996.tb01451.x>.

- Jin, K. et al. (2012) 'Design and Fabrication of Gecko-Inspired Adhesives', *Langmuir*, 28(13), pp. 5737–5742. Available at: <https://doi.org/10.1021/la204040p>.
- Jin, K. et al. (2014) 'Biomimetic Bidirectional Switchable Adhesive Inspired by the Gecko', *Advanced Functional Materials*, 24(5), pp. 574–579. Available at: <https://doi.org/10.1002/adfm.201301960>.
- Johnston, I.D. et al. (2014) 'Mechanical characterization of bulk Sylgard 184 for microfluidics and microengineering', *Journal of Micromechanics and Microengineering*, 24(3), p. 035017. Available at: <https://doi.org/10.1088/0960-1317/24/3/035017>.
- Murphy, M.P., Kim, S. and Sitti, M. (2009) 'Enhanced Adhesion by Gecko-Inspired Hierarchical Fibrillar Adhesives', *ACS Applied Materials & Interfaces*, 1(4), pp. 849–855. Available at: <https://doi.org/10.1021/am8002439>.
- Parness, A. et al. (2009) 'A microfabricated wedge-shaped adhesive array displaying gecko-like dynamic adhesion, directionality and long lifetime', *Journal of the Royal Society, Interface*, 6(41), pp. 1223–1232. Available at: <https://doi.org/10.1098/rsif.2009.0048>.
- Prusa, J. (2021) 'Original Prusa SL1S SPEED is here: Introducing the fastest desktop SLA 3D printer', *Original Prusa 3D Printers*, 16 June. Available at: [https://blog.prusa3d.com/introducing-slls\\_fastest\\_desktop\\_sla\\_3d\\_printer\\_51436/](https://blog.prusa3d.com/introducing-slls_fastest_desktop_sla_3d_printer_51436/) (Accessed: 15 November 2023).
- Purtov, J. et al. (2018) 'Improved development procedure to enhance the stability of microstructures created by two-photon polymerization', *Microelectronic Engineering*, 194, pp. 45–50. Available at: <https://doi.org/10.1016/j.mee.2018.03.009>.
- Raut, H.K. et al. (2018) 'Gecko-Inspired Dry Adhesive Based on Micro–Nanoscale Hierarchical Arrays for Application in Climbing Devices', *ACS Applied Materials & Interfaces*, 10(1), pp. 1288–1296. Available at: <https://doi.org/10.1021/acsami.7b09526>.
- Tian, Y. et al. (2006) 'Adhesion and friction in gecko toe attachment and detachment', *Proceedings of the National Academy of Sciences*, 103(51), pp. 19320–19325. Available at: <https://doi.org/10.1073/pnas.0608841103>.
- Tricinci, O. et al. (2018) 'Approximating gecko setae via direct laser lithography', *Smart Materials and Structures*, 27(7), p. 075009. Available at: <https://doi.org/10.1088/1361-665X/aa9e5f>.
- Yu, J. et al. (2012) 'Friction and Adhesion of Gecko-Inspired PDMS Flaps on Rough Surfaces', *Langmuir*, 28(31), pp. 11527–11534. Available at: <https://doi.org/10.1021/la301783q>.
- Zhang, Y. et al. (2016) 'Fabrication and Characterization of Gecko-inspired Dry Adhesion, Superhydrophobicity and Wet Self-cleaning Surfaces', *Journal of Bionic Engineering*, 13, pp. 132–142. Available at: [https://doi.org/10.1016/S1672-6529\(14\)60167-0](https://doi.org/10.1016/S1672-6529(14)60167-0).
- Zhang, Y. et al. (2021) 'Gecko's Feet-Inspired Self-Peeling Switchable Dry/Wet Adhesive', *Chemistry of Materials*, 33(8), pp. 2785–2795. Available at: <https://doi.org/10.1021/acs.chemmater.0c04576>.